CARBON 84 (2015) 124–129

Available at www.sciencedirect.com

ScienceDirect

journal homepage: www.elsevier.com/locate/carbon

Graphene based ballistic rectifiers

Arun K. Singh [a,b,*], Gregory Auton [c], Ernie Hill [c], Aimin Song [a,d,*]

[a] School of Electrical and Electronic Engineering, The University of Manchester, Manchester M13 9PL, United Kingdom
[b] Department of Electronics and Communication Engineering, PEC University of Technology, Sector-12, Chandigarh 160012, India
[c] Manchester Centre for Mesoscience and Nanotechnology, The University of Manchester, Manchester M13 9PL, United Kingdom
[d] School of Physics, Shandong University, Jinan 250100, China

ARTICLE INFO

Article history:
Received 21 July 2014
Accepted 30 November 2014
Available online 4 December 2014

ABSTRACT

Despite having the longest mean-free-path of carriers in all electronic materials, it has been virtually impossible to demonstrate graphene ballistic devices due to the rather diffusive and hence random scattering of carriers from the edges. Hence we show that this may not be true in the nonlinear transport regime in a nanodevice called ballistic rectifier. In contrast to a conventional transistor, the ballistic rectifier does not necessarily require a sizable bandgap. Here, we not only demonstrate rectifying effect at room temperature but also indicate that the carrier scattering from graphene edges in the nonlinear regime may be more specularly than previous discovered in the linear regime.

1. Introduction

Graphene, a single layer of carbon atoms arranged in a 2-D honeycomb lattice, has excellent electronic, mechanical, thermal, and optoelectronic properties [1]. These properties have recently attracted immense interest to use graphene as a potential electronic material [2]. To date, novel approaches have been employed to overcome the bottleneck of graphene in transistors, namely generating a suitable bandgap while preserving high carrier mobilities [3]. However, it may take longer before graphene transistors with the high on/off ratios, operating speed, reliability, and manufacturability required for commercialization can be realized. In contrast, the functionality of a high speed graphene based nano-rectifier, also known as ballistic rectifier [4], does not necessarily require a sizable bandgap and/or a multi-layer structure. Such a device would greatly benefit from the extremely long carrier mean-free-path in graphene. However, graphene has very different edge properties compared with conventional semiconductors. In the previous ballistic rectifier fabricated from GaAs semiconductor, the regions close to (~100 nm in GaAs) the edges of the etched areas are depleted due to the surface states on the etched sidewalls, hence forming a smooth effective boundary for the ballistic carriers to reflect from specularly [4]. However, in graphene there should be no such depletion region, because it has no band gap and instead it is speculated that the edge of the graphene will follow the lines of the crystal planes creating uneven lines of alternating zig-zag and armchair arrangements [5]. Much of the previous work suggests that any scattering at a graphene edge will be diffusive as appose to the specular scattering that is thought to be necessary for ballistic devices [6]. These studies were so far rather conclusive in the linear transport regime where the applied bias was small. As a nonlinear device, the ballistic rectifier that relies entirely on the specular scattering of carriers from the edges shall be ideal to examine the edge scatterings in graphene beyond the linear regime.

The ballistic rectifier is made of a nanoscale cross junction with or without triangular antidot (an artificial scatterer) at the center [4,7,8]. The active part of the ballistic rectifier can

* *Corresponding authors at:* School of Electrical and Electronic Engineering, The University of Manchester, Manchester M13 9PL, United Kingdom.
E-mail addresses: arun@pec.ac.in (A.K. Singh), a.song@manchester.ac.uk (A. Song).
http://dx.doi.org/10.1016/j.carbon.2014.11.064
0008-6223/

be fabricated by using nanolithography in only a single step. As a single device its full-wave rectifying functionality resembles to that of a bridge rectifier, which however requires four individual diodes [4]. The ballistic rectifier device concept differs from all conventional rectifiers because it does not contain and rely on any doping junction or barrier structures along the direction of electrical conduction. As a result, zero-threshold voltage can be achieved, thus eliminating the need for a bias circuit [9]. The zero-threshold property of ballistic rectifier further enables the elimination of the flicker noise, which often limits the microwave detection sensitivity of diode detectors particularly the so-called noise-equivalent power (NEP) [10]. The nonlinear voltage–current characteristic is instead of a direct result of intentionally broken device symmetry at the center [4]. In ballistic rectifier, charge carriers move freely without any or many scattering events in the active area of the device and are only scattered by the tailored geometry due to small dimensions, resulting in ballistic or at least quasi-ballistic transport at room temperature [11]. The planar nature of these devices means that the electrical contacts are placed side by side rather than on top of each other, which greatly reduces the parasitic capacitance and enables very high operating speeds at room temperature. With this low capacitance and ballistic carrier transport, it is possible to develop the ballistic rectifier as a possible high-speed microwave and/or terahertz (1 THz = 1000 GHz) detector as envisaged by Monte Carlo simulations [12]. Such devices have been demonstrated experimentally, performing up to the microwave frequencies of 50 GHz using InGaAs semiconductors at room temperature [13]. Details of the working principle of the ballistic rectifier in nonlinear regime can be found elsewhere [4,11].

The device speed generally scales up with the carrier mobility. Novel two-dimensional materials, in particular, graphene, are ideal to be utilized for the fabrication of ballistic rectifiers to take the advantage of the potentially ultra-high mobility and long mean-free-path even at room temperature [14]. Due to such high mobility, graphene based ballistic rectifiers are expected to work at THz frequencies. Moreover, this device has a single-layered architecture that is ideally-suited to use graphene as an active layer. Here, we report on the fabrication of two different geometries of ballistic rectifier, i.e., with and without a scatterer at the center, by using mechanically exfoliated monolayer graphene flakes. The nonlinear electrical properties have been characterized at room temperature and discussed by using a scattering approach of multi-terminal ballistic transport.

2. Device fabrication

The monolayer graphene used in this study for the fabrication of ballistic rectifiers is deposited by mechanical exfoliation technique onto a thermally grown 290 nm thick silicon oxide (SiO_2) on a highly doped silicon substrate. The *p*-doped silicon substrate is used as a global back gate to tune the Fermi energy of the device which in turn controls the carrier concentration in the graphene. The graphene flakes are identified by using an optical microscope and patterned into Hall-bar geometry by employing electron-beam lithography and oxygen-plasma etching. The ohmic contacts of Cr/Au (3 nm/40 nm) on graphene are e-beam evaporated and then the lift-off process is performed in hot acetone. The minimum conductivity (σ) is observed at the neutrality point with a back-gate voltage (V_{BG}) of −4 V, which indicates little extrinsic doping, approximately 2.9×10^{11} cm^{-2}. At small carrier concentrations, the slope of σ as a function of V_{BG} yields mobility for holes and electrons of 1572 and 1810 cm^2/Vs, respectively, which is typical on untreated SiO_2 substrates [5]. From our measured results, using a semi-classical relation [5], the estimated mean-free-path length $\lambda = (h/2e)\mu(n/\pi)^{1/2}$ for holes and electrons with a typical carrier concentration n of 2.23×10^{12} cm^{-2} are about 27 and 31 nm, respectively. Here h is Planck's constant, e is electron charge, and μ denotes the carrier mobility. The schematic diagrams of the active central region of the ballistic rectifiers with and without triangular antidot are shown in Fig. 1a and b, respectively, the dark areas represent the etched regions. The four terminals of the device, source (*S*), drain (*D*), upper (*U*), and lower (*L*), are denoted in each device. The arrows indicate the typical directions of flow of the charge carriers from *S* or *D* to *L* terminal. Fig. 1c shows a scanning electron micrograph of a typical ballistic rectifier with a triangular antidot at the center. The lithographic channel width for *S* and *D* is 50 nm while the channel width for *U* and *L* is 220 nm. The triangular antidot had an upper side length and a height of 70 nm. The typical atomic-force microscopic (AFM) image of a ballistic rectifier without artificial scatterer is shown in Fig. 1d. The effective channel width of *S*, *D* and *U* channel is 70 nm each.

3. Results and discussions

Conventional rectifying diodes are generally based on either *p*–*n* doped junction or a Schottky barrier. The built-in electric field or a threshold voltage in these devices requires an applied bias high enough to overcome the internal field and generate a significant current flow. In contrast, the ballistic rectifier has no intrinsic threshold or turn-on voltage because there is no *p*–*n* junction or Schottky barrier along the direction of electrical current in the device [4]. It is interesting to note that the ballistic rectifier relies only on symmetry breaking on the nanometer scale, which enables a unique property of absence of any threshold. When the graphene is back gated into the *n*-type region and a DC current I_{SD} is applied between the *S* and *D* terminals, the ejected electrons from *S* or *D* are deflected by a triangular antidot to the terminal *L* as indicated by the typical trajectories in Fig. 1a. Therefore, electrons are accumulated in the lower terminal of the ballistic rectifier; as a result a negative V_{LU} is induced between the *L* and *U* terminals. Correspondingly, when holes are the majority charge carriers, the induced voltage between *L* and *U* terminals is positive. On the other hand, in the ballistic rectifier without an artificial antidot at the center as shown in Fig. 1b, the two narrow channels connecting *S* and *D*, slanted by 30° from the perpendicular axis of the longitudinal channel between *L* and *U*, are responsible for the rectifying effect from the device [8]. The carrier transport in nanoscale graphene ballistic rectifiers, where the electron mean-free-path is much longer than the active region of the device, can be explained using

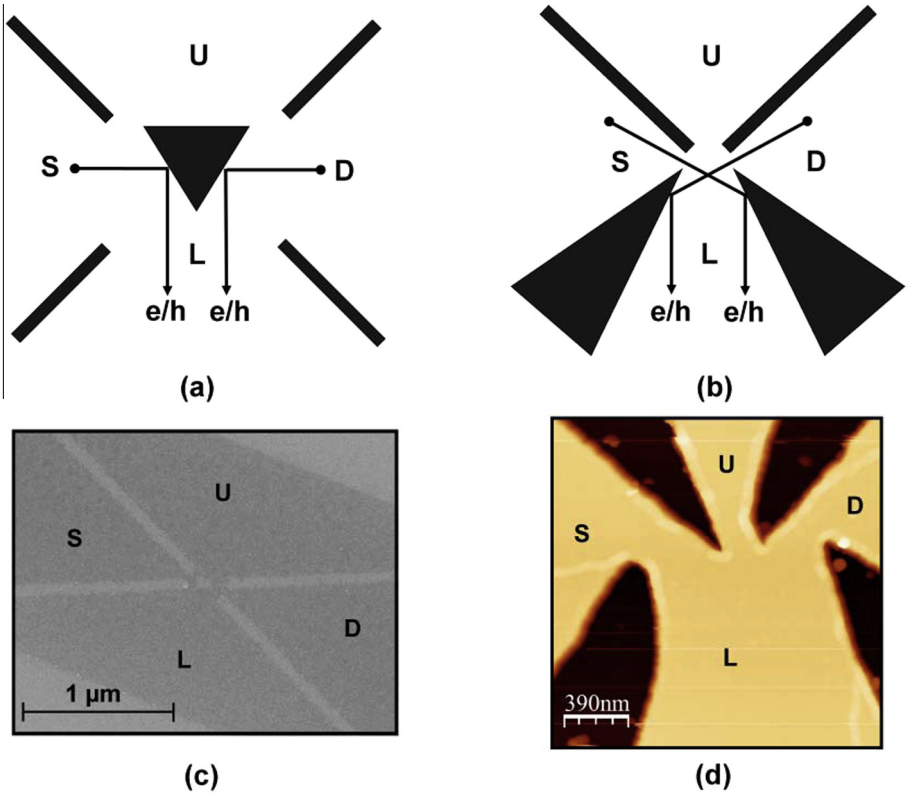

Fig. 1 – The schematic illustration of the different geometries of ballistic rectifiers (a) with and (b) without a triangular antidot, an artificial scatterer, at the center of device active region. The dark areas represent the etched regions. Arrows indicate the typical directions of flow of the charge carriers from *S* or *D* to *L* terminal. (c) The typical scanning electron microscope image (c) and atomic-force micrograph (d) of the devices with and without a triangular antidot, respectively.

an extended Büttiker–Landauer formalism. The nonlinear voltage–current characteristic exhibits a quadratic response as described by [15]:

$$V_{LU} = -\frac{3\pi\hbar}{4e^3 E_F N_{SD} N_{LU}} I_{SD}^2 \quad (1)$$

where V_{LU} is the output voltage between *L* and *U*, I_{SD} is the input current flowing between *S* and *D*, $\hbar$ is the reduced Planck's constant, *e* is the charge of an electron, E_F is the Fermi energy, N_{SD} is the number of propagating modes in *S* and *D* channels, and N_{LU} represents the number of propagating modes in *L* and *U* channel. It is evident from Eq. (1) that the V_{LU} is independent of temperature even at very small input signal to that of a conventional device. The room temperature voltage–current characteristic at $V_{BG} = 0$ V of the ballistic rectifier with a triangular antidot at its center is shown in Fig. 2a. For a real device as shown in the insets of Figs. 1c and d, lithography may not be perfect which leads to the asymmetric voltage–current response about $I_{SD} = 0$ as reported earlier in Ref. [4]. However, the overall downwards bending of the curve indicates a rectifying behavior if an AC current is applied to the *S* and *D* electrodes. The maximum nonlinear behavior from the device without antidot scatterer is observed at the back-gate voltage of −15 V as shown in Fig. 3a, where the dominant charge carriers are holes. As expected, the device exhibited geometrically induced rectifying effect. Using Eq. (1), the theoretically predicted quadratic nonlinear characteristic of the device for the range of applied I_{SD} at the back-gate voltage of −15 V, where *n* is 1.1×10^{12} cm^{-2}, is very well fitted to the experimental results in Fig. 3a. Fig. 3b shows the output voltage V_{LU} measured as a function of input current I_{SD} at a back-gate voltage of −20 V and 0 V at room temperature. A change of sign from positive to negative is observed in the output voltages when the majority charge carriers are tuned from holes (V_{BG} = −20 V) to electrons ($V_{BG} = 0$ V). Since the device dimensions are larger than the electron mean-free-path length, only a small portion of the charge carriers can travel without being scattered by random impurities or phonons; hence of ballistic or quasi-ballistic transport [16]. Nevertheless, both devices have exhibited very well the square-law behavior at room temperature. This implies that carrier scattering from graphene edges in the nonlinear regime may be far more specularly than previous discovered in the linear regime [17–20]. Understanding of such carrier scattering in the nonlinear regime will need in-depth theoretical studies, while fabricating graphene on more suitable substrates such as hexagonal boron nitrite (h-BN) to enable improved carrier mobility up to 40,000 cm^2 V^{-1} s^{-1} [21,22] and mean-free-path over 1 μm [5] shall offer further information on the edge scatterings.

To understand the observed ballistic rectifying effect in our structures that are much larger than the apparent mean-free-path, we note that most previous work on ballistic transport has been in the linear regime and at low tempera-

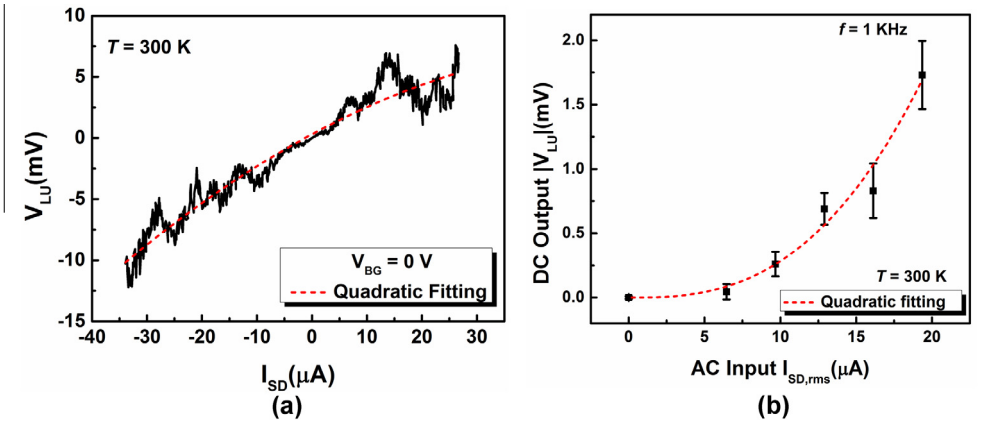

Fig. 2 – (a) V_{LU} vs I_{SD} at V_{BG} = 0 V for ballistic rectifier with triangular antidot at T = 300 K. (b) The rectified DC output voltage, based on 100 readings measured at room temperature, with respect to AC input current.

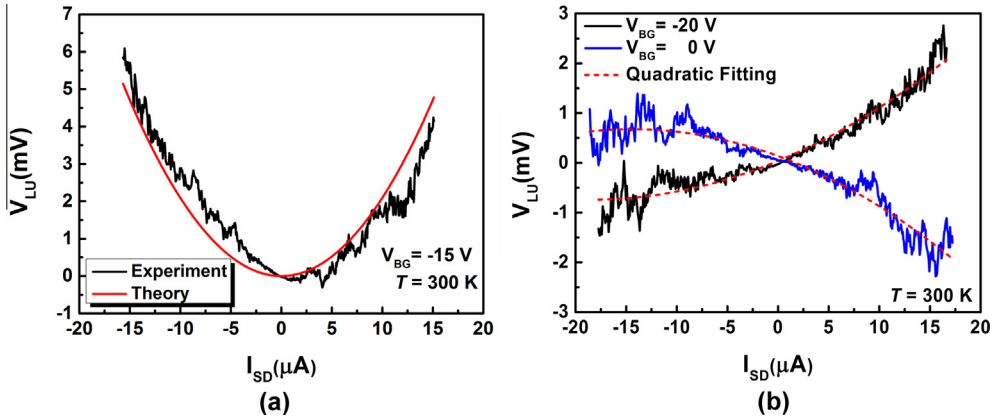

Fig. 3 – (a) Room temperature voltage–current characteristics of the ballistic rectifier without antidot scatterer at the back-gate voltage of −15 V, perfectly fits to the theoretically calculated using (1). To the left (−20 V) or right (0 V) of the neutrality point the rectified output voltage is of positive or negative sign, respectively and is in quadratic fit to the input (b).

tures. In these cases, the carrier mean-free-path extracted from the mobility needs to be larger or at least comparable to the device feature size in order to ensure ballistic or quasi-ballistic transport. However, in the nonlinear regime, the mean-free-path can be significantly enhanced by the bias voltage. Such an effect has been observed and quantitatively modeled at room temperature in InGaAs devices and silicon devices with a dimension more than one order of magnitude longer than the mean-free-path that is calculated from carrier mobility in the linear regime [23,24].

Eq. (1) shows that the quadratic response of the device should depend on the carrier density and hence the back-gate voltage. More voltage–current characteristics of the ballistic rectifier without antidot scatterer have been shown in Fig. 4 at different back-gate voltages of −30, −10, and +20 V. The data seems to be in qualitative agreement with the theory. According to Eq. (1), the output voltage will reduce as the carrier density becomes high, which was indeed as observed at gate voltages of −30 V and +20 V in Fig. 4. However, there is also a difference in the region close to the Dirac point due to the nature of graphene. In a conventional semiconductor, Eq. (1) predicts that the output voltage would increase rapidly as the carrier density reduces. However, in graphene, the zero

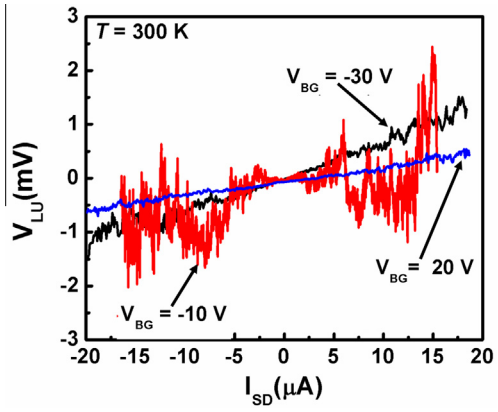

Fig. 4 – Voltage–current characteristics of the ballistic rectifier without antidot scatterer at the different back-gate voltages of −30, −10, and +20 V.

or low bandgap means that there is a co-existence of both electrons and holes around the Dirac point. Since the electrons and holes would produce output voltages of opposite signs, the device output is expected to reach a minimum,

which was indeed observed in our experiments (see the curve at gate voltage of −10 V in the new Fig. 4).

The specular scattering as indicated by the experimental results may also appear to be a bit surprising. However, we note that the previous experiments to show non-specular scattering at graphene edges were performed in the linear regime. It has been established that the electron transport in graphene nanochannels tends to be strongly influenced by random edge (arm chairs or zig-zag) and the termination of dangling bonds which result in strongly localized states/wave functions, and also Coulomb charging effect [25–27]. In the nonlinear regime, it is possible that the large applied bias provides high enough energy for the electrons or holes to reach and be subsequently trapped at the localized edge states, in a way similar to the trapped electrons at surface states in a conventional semiconductor. These bias-induced trapped charges can then produce long-range Coulomb field to scatter away other incoming carriers, forming effectively a depletion region close to the edge which is also similar to that in a conventional semiconductor. As a result, the carriers may be scattered away at a distance from the disordered edges, resulting in more specular scatterings than in the linear regime.

Apart from the ballistic rectifying effect, thermopower in nanostructures may also produce quadratic voltage or current in the transverse direction. Thermopower has been studied in nano-channels based on conventional semiconductors and graphene [28,29]. It is also indeed true that thermopower effect in our structure, if significant, would produce a quadratic output. However, for *n*-type carrier transport, the thermopower effect is expected to generate a negative voltage in the *U* terminal with respect to the wider *L* terminal, which is the opposite to what we have observed. In the case of the hole transport, the observed output in our device is also the opposite to what would be expected from the thermopower effect. Therefore, it can be concluded that the thermopower effect, if any, is far less dominant than the ballistic rectifying effect in our experiment.

It is interesting to note that the experimental voltage–current curves in Figs. 2–4 are relatively noisy. This is partially due to the fact that the devices were measured at room temperature (hence more thermal noise) and on a probe station rather than in a screened cryostat. The experimental data shows that the noise is actually quite low in the low-bias linear regime. The noise level increases rapidly with the applied voltage. This indicates the dominant noise being the low-frequency flicker noise, which may well be due to the interface scattering at the SiO_2 surface.

In order to characterize the rectification properties of the ballistic rectifier an AC current at 1 kHz is applied between *S* and *D* of the device with a triangular antidot and the induced DC output voltage is measured simultaneously between *L* and *U* as shown in Fig. 2b at the room temperature. Due to the conducting Si substrate, the devices are not suitable for operation at GHz/THz frequencies. The error bars are based on 100 readings of the output DC voltage. The device exhibited a quadratic response to the input current meaning that the DC output voltage is a linear function of applied AC power, hence follows the square-law response [13]. The measured results in Fig. 2b yield the voltage responsivity (β_V), which is a detection sensitivity of the microwave detector, to be around 66.68 mV/mW. However, the maximum intrinsic voltage responsivity is estimated to be around 110.92 mV/mW from the nonlinear V_{LU}–I_{SD} characteristic in Fig. 2a considering the device impedance of 55 kΩ at V_{BG} = 0 V. The noise-equivalent power, which determines the minimum possible power a detector can resolve, is proportional to thermal noise of the device. The estimated NEP for both devices is in the order of 10^{-9} W/Hz$^{1/2}$, comparable to that of a commercially available uncooled THz detector such as bolometer and Goley cell, etc. [30]. More importantly, the capability to preform direct rectification rather than responding to heat enables a very fast response time as a detector.

4. Conclusion

Nonlinear transport at room temperature in graphene based ballistic rectifiers with different geometries, i.e., with and without triangular anti-dot at the center of nanoscale cross junction, has been investigated for the first time. Different from previous devices based on conventional semiconductors, both positive and negative signs of output voltage have been observed for *p*- and *n*-type charge carriers, respectively. In contrast to *p*–*n* junctions or Schottky barrier diodes, these devices have demonstrated a square-law operation, zero-bias rectification at room temperature. We estimate that the ballistic rectifiers fabricated with graphene on optimum substrates to achieve the much higher intrinsic motility to ensure purely ballistic transport may improve the responsivity and hence NEP by about two orders of magnitude. The nonlinearity of the device characteristic, its intrinsic zero threshold voltage, high operating speed, and ease of integration with planar rectennas will potentially make them suitable for a range of microwave/THz applications such as communications, detection, and imaging.

Acknowledgements

The authors thank to F. Schedin for technical support. The work was supported by NSFC (No. 11374185) and EU FP7 (No. 243845) grants. A.K.S. acknowledges the financial support of the Ministry of Social Justice and Empowerment, Government of India and PEC University of Technology, Chandigarh, India.

REFERENCES

[1] Castro Neto AH, Guinea F, Peres NMR, Novoselov KS, Geim AK. The electronic properties of graphene. Rev Mod Phys 2009;81(1):109–62.
[2] Liao L, Duan X. Graphene for radio frequency electronics. Mater Today 2012;15(7–8):328–38.
[3] Schwierz F. Graphene transistors: status, prospects, and problems. Proc IEEE 2013;101(7):1567–84.
[4] Song AM, Lorke A, Kriele A, Kotthaus JP, Wegscheider W, Bichler M. Nonlinear electron transport in an asymmetric microjunction: a ballistic rectifier. Phys Rev Lett 1998;80:3831–4.
[5] Mayorov AS, Gorbachev RV, Morozov SV, Britnell L, Jalil R, Ponomarenko LA, et al. Micrometer-scale ballistic transport

in encapsulated graphene at room temperature. Nano Lett 2011;11(6):2396–9.
[6] Masubuchi S, Iguchi K, Yamaguchi T, Onuki M, Arai M, Watanabe K, et al. Boundary scattering in ballistic graphene. Phys Rev Lett 2012;109:036601.
[7] Song AM, Lorke A, Kotthaus JP, Wegscheider W, Bichler M. Experimental and theoretical studies on nonlinear transport in ballistic rectifiers. Jerusalem (Israel): The 24th international conference on the physics of semiconductors (ICPS 24); 1998. p. 1–4.
[8] Koyama M, Fujiwara K, Amano N, Maemoto T, Sasa S, Inoue M. Electron transport properties in InAs four-terminal ballistic junctions under weak magnetic fields. Phys Status Solidi C 2009;6(6):1501–4.
[9] Song AM, Manus S, Streibl M, Lorke A, Kotthaus JP, Wegscheider W, et al. A nonlinear transport device with no intrinsic threshold. Superlattices Microstruct 1999;25(1–2):269–72.
[10] Singh AK, Kasjoo SR, Song AM. Low-frequency noise of a ballistic rectifier. IEEE Trans Nanotechnol 2014;13(3):527–31.
[11] Song AM. Room-temperature ballistic nanodevices. Encycl Nanosci Nanotechnol 2004;9:371–89.
[12] Vasallo BG, González T, Pardo D, Mateos J. Monte Carlo analysis of four-terminal ballistic rectifiers. Nanotechnology 2004;15:S250–3.
[13] Song AM, Omling P, Samuelson L, Seifert W, Shorubalko I, Zirath H. Operation of InGaAs/InP-based ballistic rectifiers at room temperature and frequencies up to 50 GHz. Jpn J Appl Phys 2001;40:L909–11.
[14] Bolotin KI, Sikes KJ, Jiang Z, Klima M, Fudenberg G, Hone J, et al. Ultrahigh electron mobility in suspended graphene. Solid State Commun 2008;146:351–5.
[15] Song AM. Formalism of nonlinear transport in mesoscopic conductors. Phys Rev B 1999;59(15):9806–9.
[16] Du X, Skachko I, Barker A, Andrei EY. Approaching ballistic transport in suspended graphene. Nat Nanotechnol 2008;3:491–5.
[17] Areshkin DA, Gunlycke D, White CT. Ballistic transport in graphene nanostrips in the presence of disorder: importance of edge effects. Nano Lett 2007;7(1):204–10.
[18] Ritter KA, Lyding JW. The influence of edge structure on the electronic properties of graphene quantum dots and nanoribbons. Nat Mater 2009;8:235–42.
[19] Mucciolo ER, Castro Neto AH, Lewenkopf CH. Conductance quantization and transport gaps in disordered graphene nanoribbons. Phys Rev B 2009;79:075407.
[20] Ouyang Y, Wang X, Dai H, Guo J. Carrier scattering in graphene nanoribbon field-effect transistors. Appl Phys Lett 2008;92:243124.
[21] Dean CR, Young AF, Meric I, Lee C, Wang L, Sorgenfrei S, et al. Boron nitride substrate for high-quality graphene electronics. Nat Nanotechnol 2010;5:722–6.
[22] Zomer PJ, Dash SP, Tombros N, van Wees BJ. A transfer technique for high mobility graphene devices on commercially available hexagonal boron nitride. Appl Phys Lett 2011;99:232104.
[23] Wallin D, Shorubalko I, Xu HQ, Cappy A. Nonlinear electrical properties of three-terminal junctions. Appl Phys Lett 2006;89:092124.
[24] Meng FT, Sun J, Graczyk M, Zhang KL, Prunnila M, Ahopelto J, et al. Nonlinear electrical properties of Si three-terminal junction devices. Appl Phys Lett 2010;97:242106.
[25] Han MY, Özyilmaz B, Zhang YB, Kim P. Energy band-gap engineering of graphene nanoribbons. Phys Rev Lett 2007;98:206805.
[26] Han MY, Brant JC, Kim P. Electron transport in disordered graphene nanoribbons. Phys Rev Lett 2010;104:056801.
[27] Ponomarenko LA, Schedin F, Katsnelson MI, Yang R, Hill EW, Novoselov KS, et al. Chaotic Dirac billiard in graphene quantum dots. Science 2008;320:356.
[28] Molenkamp LW, van Houten H, Beenakker CWJ, Eppenga R, Foxon CT. Quantum oscillations in the transverse voltage of a channel in the nonlinear transport regime. Phys Rev Lett 1990;65:1052.
[29] Zuev YM, Chang W, Kim P. Thermoelectric and magnetothermoelectric transport measurements of graphene. Phys Rev Lett 2009;102:096807.
[30] Sizov F, Rogalski A. THz detectors. Prog Quant Electron 2010;34:278–347.